Journal Name

ARTICLE

What do we actually see in intracellular SERS? Investigating nanosensor-induced variation

Received 00th January 20xx,
Accepted 00th January 20xx

DOI: 10.1039/x0xx00000x

www.rsc.org/

J. Taylor[a], J. Milton[b], M. Willett[c], J. Wingfield[d] and S. Mahajan[a]*

Plasmonic nanoparticles (NPs), predominantly gold (AuNPs), are easily internalised into cells and commonly emloyed as nanosensors for reporter-based and reporter-free intracellular SERS applications[1]. While AuNPs are generally considered non-toxic to cells, many biological and toxicity studies report that exposure to NPs induces cell stress through generation of reactive oxygen species (ROS) and upregulated transcription of pro-inflammatory genes, which can result in severe genotoxicity and apoptosis[2]. Despite this, the extent to which normal cellular metabolism is affected by AuNP internalisation remains a relative unknown along with the contribution of the uptake itself to the SERS spectra obtained from within so called 'healthy' cells, as indicated by traditional viability tests. This work aims to interrogate the perturbation created by treatment with AuNPs under different conditions and the corresponding effect on the SERS spectra obtained. We characterise the changes induced by varying AuNP concentrations and media-serum compositions using biochemical assays and correlate them to the corresponding intracellular reporter-free SERS spectra. The different serum conditions lead to different extents of nanoparticle internalisation. We observe that changes in SERS spectra are correlated to increasing amount of internalisation, confirmed qualitatively and quantitatively by confocal imaging and ICP-MS analysis, respectively. We analyse spectra and characterise changes that can be attributed to nanoparticle induced changes. Thus, our study points to the need to understand condition-dependent NP-cell interactions and standardisation of nanoparticle treatments to establish the validity of intracellular SERS experiments and for use of the methodology for all arising applications.

Introduction

The biocompatibility offered by plasmonic gold nanoparticles (AuNPs) is one of the major advantages of their use in intracellular SERS experiments. Employed as SERS probes, their applications include monitoring of cellular functions[3,4], dynamics[5–7], enzyme kinetics[8,9], stress response[10–13], apoptosis and cell death[11,14,15] along with probing specific compartments such as the mitochondria[16] and tracking of drugs released into the cytoplasm by NP carriers[17–20]. Cellular uptake is achieved through voluntary incorporation into living cells by endocytotic mechanisms, following a simple incubation period with NP-doped cell culture media. Although the explicit mechanism depends on several parameters such as NP size, surface charge/coating and cell type, it is accepted that NPs are internalised by cells into endosomal transport vesicles following the adherence of extracellular serum proteins to their surface to form a biocompatible 'protein corona' around the inorganic NP. The make-up of the protein corona gives an NP its biochemical identity as experienced by cells and thus affects both uptake and intracellular localisation[21–23]. It is subject to dynamic changes in composition and thickness (usually measured between 3-15 nm) depending on the media in which it is suspended[24,25]. Initial formation of the corona occurs rapidly upon contact and in the case of culture medium, a stable and biocompatible structure is formed which lowers the free energy of NP-membrane interaction[22,24,26,27]. Functionalisation of NP surface may also be performed with cell penetrating agents to achieve direct localisation towards the cytosol or desired organelles, evading removal by exocytosis for probing a diverse range of intracellular targets[28]. For details on approaches to intracellular SERS the role of NPs as SERS probes the reader is directed to published exhaustive reviews[1,29–31].

Despite reports that NPs (particularly AuNPs) of SERS relevant diameter (20-100 nm) are non-toxic to cells, typically evidenced by traditional cell viability tests such as trypan blue or MTT (3-(4,5-dimethylthiazol-2-yl)-2,5-diphenyltetrazolium bromide) assays, their nanotoxicity is often discussed/questioned[2,21,32,33]. Much debate arises from not only inconsistencies in the manner in which intracellular SERS experiments are performed and reported, but also from the sheer complexity of NP-cell interactions. For instance, toxicity depends on features such as cell phenotype, NP material, size, morphology, concentration, surface charge and modifications. Despite this, the accepted consensus is that NPs, particularly Au nanospheres, have negligible effect on cell viability as shown by the traditional, biological assays.

[a] Department of Chemistry and Institute of Life Sciences (IfLS), University of Southampton, United Kingdom, SO17 1BJ.
[b] Ocean and Earth Sciences, University of Southampton, SO14 3ZH
[c] Biological Sciences, University of Southampton, United Kingdom, SO17 1BJ.
[d] Discovery Sciences, Screening and Compound Management, AstraZeneca, Unit 310 - Darwin Building, Cambridge Science Park, Milton Road, Cambridge, United Kingdom, CB4 0WG.
*Corresponding author email: s.mahajan@soton.ac.uk

Electronic Supplementary Information (ESI) available: Nanoparticle uptake data for optimisation of incubation time, SERS data with different acquisition times, *in vitro* control SERS spectra and tables with detailed peak assignments. See DOI: 10.1039/x0xx00000x

The property of being non-toxic does not however rule out that uptake of bulky, inorganic cargo such as AuNPs can impact molecular-level homeostatic mechanisms of living cells. Particularly implicated with exposure to NPs is oxidative stress, defined as an imbalance between cellular production of reactive oxygen species (ROS) and antioxidant defences[2,34–36]. ROS, such as $\cdot O_2^-$, ·OH and H_2O_2, production is a normal cellular process which performs roles in cell signalling and immunodefence. However, such species also inflict damage upon macromolecules like proteins, lipids and DNA when production surpasses the level which are counterbalanced by the action of antioxidants such as glutathione and superoxide dismutase[37]. Oxidative stress related effects observed following inorganic NP internalisation include increased ROS generation, decreased mitochondrial membrane potential, lipid peroxidation and decreased activity of enzymatic antioxidants[2]. DNA damage is also commonplace, exhibiting chromosomal fragmentation, DNA strand breakages and induced gene mutations[2,38,39]. The response to DNA damage involves either initiation of DNA repair mechanisms or invoking cell cycle arrest and apoptosis in extreme cases, involving biological pathways implicated in oxidative and cell stress[34,40,41].

SERS has recently been applied to achieve ratiometric sensing of oxidative stress in live cells using a SERS-reporter based platform by gold nanoflowers functionalised with 4-mercaptophenol (4-MP) reporter molecules[13]. The probe was tailored specifically to the ROS/antioxidant pair hypochlorite (ClO^-) and glutathione (GSH), indirectly detecting heightened ClO^- levels by its binding to 4-MP and subsequent alterations in SERS signature, with recovery of the initial spectrum achieved following treatment with GSH[13]. Similarly, organic Raman reporter molecules have been chemisorbed onto Au nanoshells to provide ratiometric, quantitative and reversible measurement of chemically-induced cellular hypoxia[42]. Evaluation of cytotoxicity of nanomaterials (ZnO, TiO_2 NPs and single-walled carbon nanotubes, SWCNTS) towards cells has also been performed using a reporter-free SERS methodology[12]. The study corroborates data obtained by WST-1 cell proliferation and Annexin V-FITC/PI apoptosis and necrosis assay, along with SERS spectra collected using co-incubated AuNPs to provide molecular level insights into the toxic events occurring upon internalisation of the nanomaterials. Inconsistencies between the two biological assays, observed in two cell lines verified their unreliable nature induced by NP-dye interactions despite careful washing of samples. More significantly, potential SERS-markers of cell stress as induced by the nanomaterials were identified, with alterations observed in peaks relating to protein structure, ratios of phenylalanine (Phe) peak intensities and redistribution of cellular endoplasmic reticulum and mitochondria[12].

Our work here however, aims to understand intracellular SERS in a fundamental manner, by observing the hugely complex cellular events induced by exposure to the nanoparticle SERS-probes themselves. While previous studies employ SERS NPs to monitor cellular oxidative stress upon induction by exposure to chemical stress agents such as TBHP or other nanomaterials, a gap exists in our knowledge of the biochemical changes induced arising from simple AuNP internalisation itself. Therefore, we administer the most ubiquitously employed SERS probes, spherical AuNPs, to human neuroblastoma cells at a range of incubation concentrations to observe spectral differences arising from wider biochemical changes induced due to exposure to nanoparticles (**Figure 1**). The effect of altering the foetal bovine serum (FBS; nutrient protein) content of the medium in which AuNPs are administered to cells is also considered, with previous reports demonstrating that reducing or removing the serum content of incubation medium results in increased cellular uptake[23]. Confocal fluorescence microscopy and inductively coupled plasma mass spectrometry (ICP-MS) are performed on cell treatments in order to visualise intracellular NP localisation and quantify their uptake, respectively. Reactive oxygen species (ROS) activity assay, dichlorofluorescein diacetate (DCF-DA) a fluorescent dye which is converted to dichlorofluorescein (DCF) in the presence of ROS to imply oxidative stress, was used to determine its manifestation following NP administration. Correlation of ROS activity with internalisation of NPs allows identification of one of the effects in the complex cellular events which unfold during NP-cell interaction and affect SERS spectra. Principal component analysis (PCA) and linear discriminant analysis (PCA-LDA) have previously been applied to SERS datasets by our group to achieve characterisation of the endolysosomal pathway[7] and distinguishing cell phenotypes[43]. In this application, we carefully apply PCA to observe alterations of cellular SERS spectra induced following various AuNP treatments to provide molecular-level detail of the changing cellular environment. These conclusions are contrasted with viability data obtained by classical trypan blue assay challenging the validity of intracellular SERS experiments based upon ‘healthy’ cells provided by simple viability assays. We finally analyse spectral changes due to increased NP internalisation to identify SERS markers of AuNP-induced cellular changes. This knowledge is fundamental to establish understanding of cellular pathways and their response to NP uptake and holds implications for circumventing issues in the development of intracellular SERS-based applications.

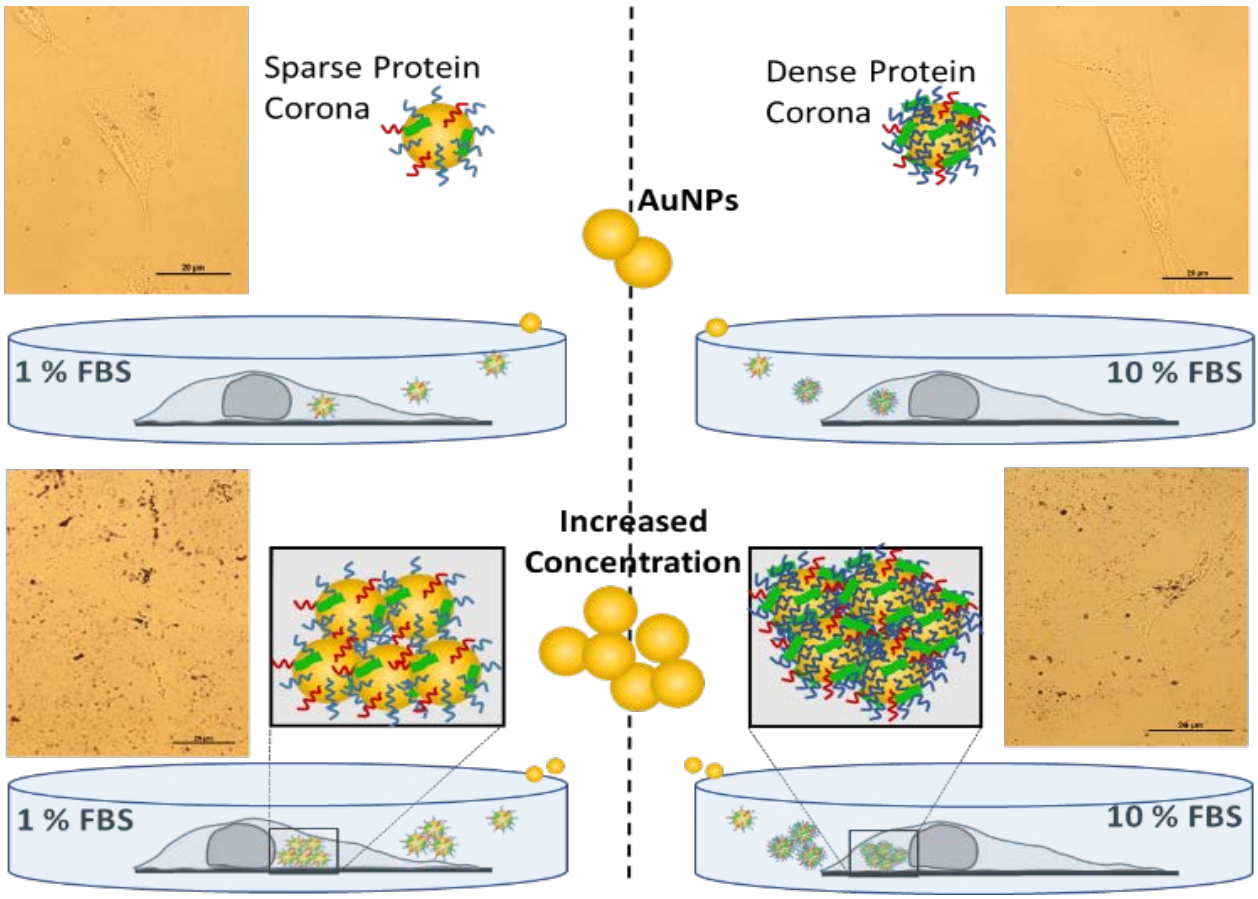

Figure 1: Schematic demonstrating incubation of SH-SY5Y cells with varying AuNP treatments and the effect of media-serum content on the protein corona formed around NPs. Uptake was visualised in brightfield images. Increased density of protein corona is reported to enhance biocompatibility although can limit cellular internalisation[23]. The degree of internalisation increases with the concentration of AuNPs administered.

Methods

Cell Culture

SH-SY5Y (human neuroblastoma cell line) cells were cultured in DMEM supplemented with 10% fetal bovine serum (FBS), 1% penicillin-streptomycin (pen-strep) mixture. Cells were incubated at 37 ^{o}C, 5% CO_2, split every 4 days and underwent regular checks to ensure freedom from mycoplasma[44]. Cells were seeded at 25000 cells onto lumox® 96 well plates (Sarstedt Ltd) and poly-L-lysine coated glass cover slips for ROS assay and SERS measurements respectively, within either culture DMEM or reduced-serum DMEM (1% FBS) including retinoic acid (RA, 10 µM) to induce neuronal differentiation over 48 h.

AuNP Administration

Following washing by phosphate buffered saline (PBS) solution, AuNP incubations were performed using 60 nm colloidal AuNPs (BBI international) at media concentrations of 250, 100, 10, 1 and 0.1 µM in DMEM (10% FBS, 1% pen-strep), as well as reduced-serum DMEM (1% FBS, 1% pen-strep), both without phenol red. The incubation was performed over 24 h to achieve maximal internalisation of AuNPs (Fig. S1). Control cells were maintained in the same media composition without AuNPs for the same time period. Following exposure, cells were washed with PBS and fixed in 4% para-formaldehyde before analysis, in a methodology similar to that previously published by our group[43]. Control AuNPs were incubated in each media composition for 24 h before washing, storage and analysis in PBS to discern the SERS signature of the NPs' protein corona microenvironment.

Cell Viability Assay

Cells were seeded at 25000 cells in 12-well plates and underwent previously outlined differentiation and AuNP administration treatments. This was followed by detachment of cells from plates using trypsin, centrifugation and resuspension of cells in a 1:1 v/v solution of culture medium and 0.4% trypan blue solution (Sigma-Aldrich). After 5 mins cells were transferred to a haemocytometer for counting of viable and non-viable cells. 2 Repeats were performed at each combination of AuNP and FBS conditions.

Confocal Fluorescence Microscopy

For visualisation of AuNPs' localisation within cells under each treatment condition, confocal microscopy was sequentially performed to observe NP scattering around fluorescently stained cells. Following AuNP incubation, cells were washed and incubated with CellTracker Red CMTPX (ThermoFisher Scientific, exc/em 577/602 nm, 10 uM, 30 mins) in DMEM free serum and phenol red. Cells were then fixed and stored in PBS before mounting in glycerol on glass slides for imaging.

Confocal laser scanning microscopy was performed with a Leica SP-8 confocal microscope. High-magnification images were obtained with a Nikon plan apochromat 63x oil-immersion objective. AuNPs were imaged in reflection mode using a 514 nm argon laser line and

PMT detection 518 – 550 nm (green) and averaged 4 times. CellTracker red fluorescence was imaged using a 561 nm solid-state laser line and PMT detection 558 – 603 nm (red), averaging twice. Z-stacking was performed with step-size of 0.33 µm. 3D and cross section images were processed using Fiji ImageJ.

Inductively coupled plasma – Mass spectrometry (ICP-MS)

Cells seeded at 25000 cells underwent the previously outlined differentiation protocol and AuNP incubation at concentrations of 0, 10, 100 and 250 µM in 1 and 10 % FBS media. Cells were washed 3 times with PBS to aid removal of extracellular NPs before being collected by trypsinisation. Suspensions of control and NP-containing cells, along with AuNP standards (10, 100, 250 µM in 1 and 10% FBS media), were digested in aqua regia (3:1 HCl:HNO3) in Teflon vessels on a hotplate for 30 h. Following digestion the samples were diluted with 5% HCl and analysed using ICP-MS.

Au measurements were carried out on a Thermo Scientific ELEMENT XR HR-ICP-MS at the University of Southampton (Ocean and Earth Science). A standard sample introduction configuration was used, namely a PFA Peltier-cooled cyclonic spray chamber (ESI) with a PFA nebuliser being pumped (at about 100µl/min) via peristaltic pump. The ICP-MS system used a Ni H-skimmer cone and Ni standard sample cone. Samples were introduced via an autosampler with a HEPA filtered enclosure (ESI SC2).

On the day of analysis the ELEMENT XR instrument was tuned for optimal sensitivity, stability and low oxide formation using a 0.1 ppb tuning solution. All data were acquired in low resolution mode to maximise sensitivity (0.5M CPS/ppb Au). The internal standard element Re (at 1 ppb) was introduced in to all samples, standards and blanks and used to correct for matrix and instrumental drift. Element/Isotopes acquired: Au [197] and Re [185].

Using the ELEMENT operating software an analysis sequence was constructed containing blanks, calibration standards (derived from 1000 ppm synthetic standards, Inorganic Ventures, Inc) and the unknown samples. All solutions were spiked with the internal standard Re. Data was acquired for the isotopes of interest in peak-jumping mode (4 x 15 second repeats per sample). After each sample analysis, a wash solution containing 5% HCl was run until background levels of all elements were achieved (typically <5 minutes). The data quality was monitored throughout the run by examination of the statistics produced after each analysis. Within each run the reproducibility was typically better than 2% RSD for the 4 repeats. The data handling procedure included the following steps: Internal correction, blank correction, calibration against 5 standards and dilution correction.

ROS Detection Assay

In parallel with the previously described AuNP incubation, cells were treated with chemical stress agent tert-butyl hydroperoxide (TBHP) as positive controls. The agent was administered for 4 h at 250 µM media concentrations as per manufacturer's (Abcam plc) instructions. Fluorogenic dye for ROS detection 2',7'-dichlorofluorescein diacetate (DCF-DA, exc/emm 495/529 nm, Abcam plc) was administered (25 µM) to TBHP treated cells and AuNP treated cells 45 mins prior to the completion of the stress treatments after thorough washing by PBS (to minimise NP-dye quenching through removal extracellular AuNPs). Fluorescence readings were recorded using a Promega GLOMAX® fluorescence plate reader and a 490/510-570 nm filter set.

Raman Microspectroscopy

Cover slips were mounted and sealed onto glass microscope slides for analysis by Raman microspectroscopy. Raman spectra were recorded using a Renishaw Raman InVia micro-spectrometer equipped with streamline accessory (Renishaw plc, Wotton-under-Edge, UK). System parameters consisted of a 633 nm point laser, Renishaw-automated 100 nm encoded XYZ stage, Rayleigh edge filter, 1200 lines/mm (1.7 cm^{-1} spectral resolution) diffraction grating dispersing Raman signals onto a master Renishaw peltier cooled charge coupled detector (1024 pixel x 256 pixel). Calibration of Raman shifts was carried out using an internal silicon wafer. A colour camera mounted on the microscope was used to obtain brightfield images (figure 1) in transmission to visualize areas for spectral acquisition. A 63x Leica water-immersion objective lens (NA = 1.20) was used. Streamline mapping utility was employed to reveal AuNP localisation across whole cells by rapid scanning for the phonon-plasmon scattering mode from gold nanoparticles which results in a Raman peak at around 150 cm^{-1} in our experiments[45]. Cellular regions exhibiting strong scattering intensities for this mode, thus highest internal concentrations of AuNP aggregates, were interrogated by point maps of 300 nm step size and either 3x 1 s or 3x 10 s exposures of typically 0.3 mW laser exposure. Both data sets show similar spectra as shown in the supporting information **Figure S2**. 72 spectra in the range 350-2150 cm^{-1} were collected from intense scattering regions across 6 cells and 2 repeats for each treatment. The broadness of some spectral features observed in class mean spectra are a natural consequence of spectral variation within cells.

Raman Spectral Processing and Multivariate Analysis

Cosmic rays were removed from the SERS spectral maps using Renishaw Wire 3.4 software. Spectra were truncated to the spectral range 350–1650 cm^{-1} before polynomial (order 5) baseline correction and wavelet denoising were performed. This data was used for plotting class mean spectra following vector normalisation.

Raman spectra provide large and complex data matrices which require sensitive decomposition algorithms to extract key features and discriminate subtle but crucial characteristics between categorised data. These are unidentifiable by univariate analysis alone, therefore IRootLab graphical user interface toolkit for MATLAB R2009a (TheMathsWorks, Natick, MA, USA) was utilised to apply multivariate analysis PCA was performed on the background subtracted and denoised spectra obtained above after mean-centring and vector normalisation[46]. PCA is an unsupervised statistical technique which reduces the dimensionality of original data to produce scores and loadings plots from derived principal components (PCs) of the mean-centred, processed spectra. The process can be simplified as a geometrical replotting of each event (spectrum) in the multidimensional dataset onto a new set of axes (PCs) to identify the greatest possible variance within it. Scores are plotted into this calculated PC space to reveal clustering of similar data (spectra) and therefore discriminate between possible classes of data. PC loadings are correlated to the original data to discern which variables (wavenumbers) are most responsible for the separation achieved by calculation of weighting coefficients of the variance. Each PC was examined individually to determine which represented the best segregation of classes and derived PC loadings identified the corresponding vibrational modes.

Results and Discussion

Cell Viability

The effect of administering SERS nanosensors at varying concentrations and within high and reduced serum media on SH-SY5Y cell viability was assessed using trypan blue assay (**Figure 2A)**. Cells incubated with AuNPs in DMEM containing 1% FBS exhibited a generally lower viability (range 96.3-85.3%) compared to those within serum-rich DMEM (96.4-91.6%). Comparison of these values with control spectra (viability 95.4 and 88.0% for 10% and 1% FBS media content respectively) confirms this to be an effect of serum content rather than AuNP exposure. This result is consistent with literature citing the use of 10% FBS media as optimal for culturing healthy SH-SY5Y cells[44]. No pattern can be identified in the results on viability of cells with 1% FBS AuNP treatments, with values fluctuating around a level matching that of control cells. 1% FBS treatments maintained a consistently high viability between controls and AuNP treatments up to 100 uM (range 96.4-94.7%). 250 uM AuNP treatments exhibited the lowest viabilities in 10% and 1% FBS contents (91.6 and 85.3% respectively), however these values are still within 3.8 and 2.7% of control cell viabilities and thus do not show a significant loss in viability following application and uptake of AuNPs.

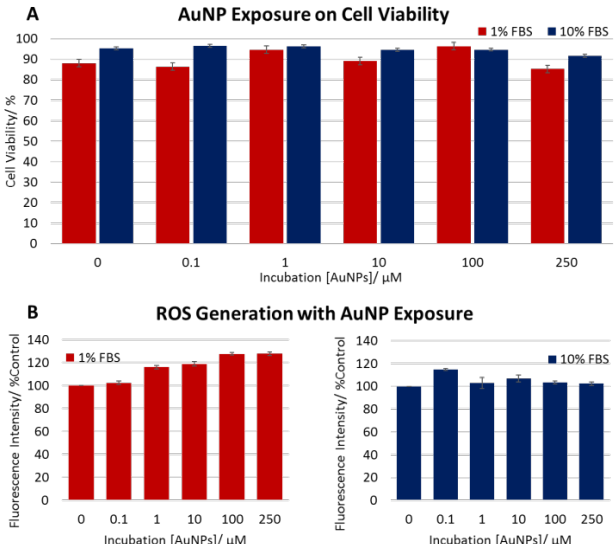

Figure 2 Effects of AuNP administration to differentiated SH-SY5Y cells at concentrations of 0.1, 1, 10, 100 and 250 µM within media containing 1 (red) and 10% (blue) FBS for 24 h, as observed by A) trypan blue cell viability and B) DCF-DA ROS detection assays.

ROS Detection by DCF-DA Assay

Cellular ROS levels were detected by DCF-DA assay and subsequent fluorescence measurements following AuNP incubation, quantified by comparison with control cells (**Figure 2B**). In all cases ROS generation was observed to be increased with AuNP treatments relative to control cells. However, cells incubated with AuNPs in 10% FBS-medium exhibited no discernible pattern in ROS levels with increased incubation concentrations of AuNPs. Treatments of 1-250 µM AuNPs displayed relatively consistent fluorescence intensities within 6.9% of control cells. Only the treatment with 0.1 µM AuNPs showed a relatively significant increase of 14.8±0.8% in ROS levels from control cells. In contrast, cells incubated with AuNPs in 1% FBS-medium showed an incremental increase in ROS generation with increased AuNP concentration. The small increase in fluorescence intensity observed with 0.1 µM AuNPs (2.5±1.5%) steadily increased to 19.0±2.0% at a 10 µM treatment which then increased by 27.6±1.0 and 27.9±1.5%, respectively at AuNP treatment concentrations of 100 and 250 µM. Thus ROS generation increased significantly with administration of increasing concentrations of AuNPs in 1% FBS media, implying enhanced degrees of oxidative stress experienced by cells following uptake of large AuNP cargos in these conditions. It is notable cells that have been administered AuNPs in 10% serum media do not show as much oxidative stress as those in 1% media. It is likely that AuNPs fed through the more concentrated 10% serum-protein rich medium have 'thicker' or more protein-like nutrient corona around them and therefore cause less stress. We also note that the trend in ROS generation caused by AuNPs in 1% FBS media is not mirrored in the measured cell viabilities. This suggests that AuNP treatment can cause changes in cell metabolism which are not captured by traditional viability tests.

Identification of NP-induced SERS Spectral Changes

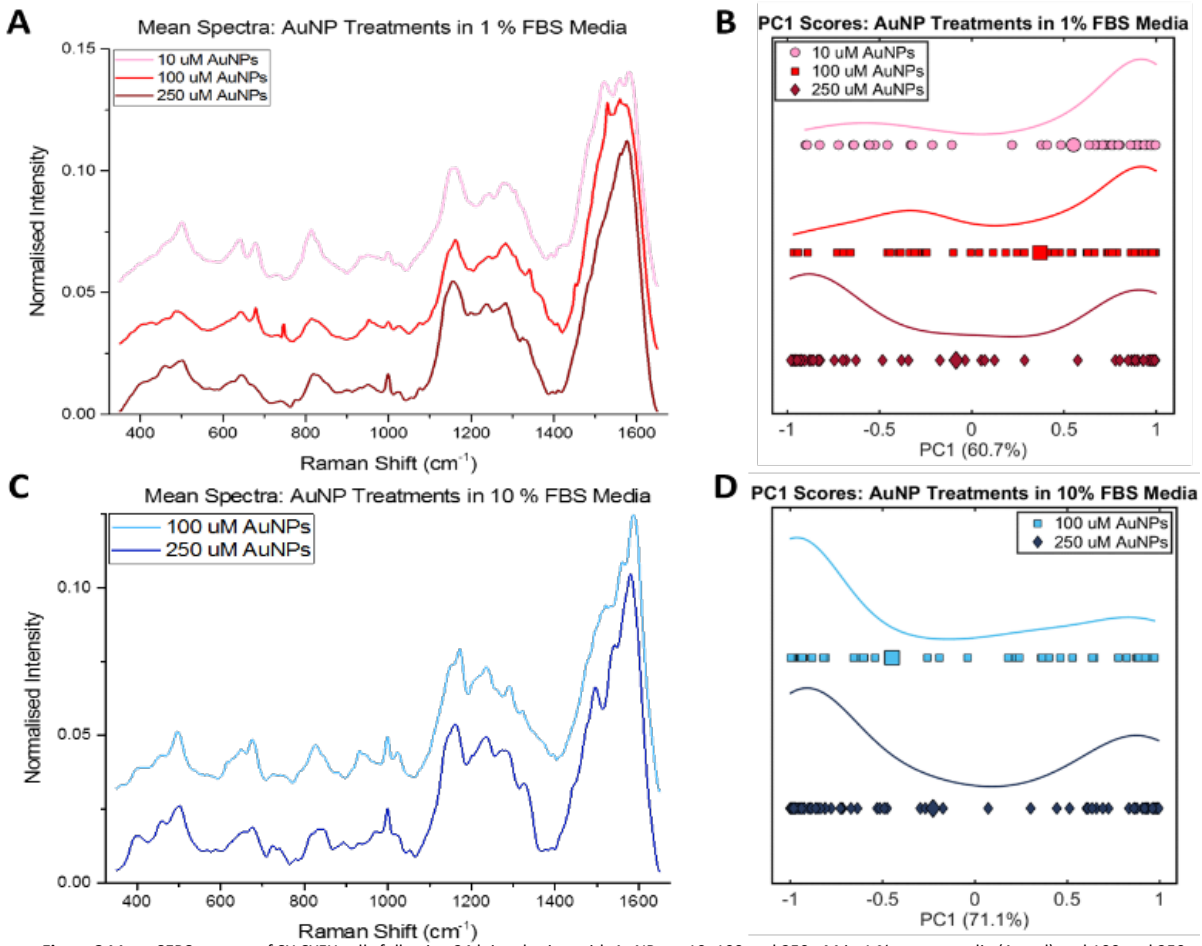

Figure 3 Mean SERS spectra of SY-SY5Y cells following 24 h incubation with AuNPs at 10, 100 and 250 µM in 1 % serum media (A, red) and 100 and 250 µM in 10 % serum media (C, blue). Classification of SERS spectra was observed by PC1 scores in an AuNP-dependent manner within 1 % media (B, red) and to a lesser extent in 10 % media (D, blue). The spectra in A and C are offset for clarity.

A total of 432 SERS spectra were acquired from cells incubated with 10, 100 and 250 µM AuNPs in 1% and 10% FBS media to explore the manifestation of spectral variation in corresponding SERS spectra. Residence of AuNPs in cells was observed to be maximal after 24 h of incubation period, so this duration was selected for use (Supporting Information **Figure S1**). The locations which gave SERS signals in cells steadily increased with AuNP concentration; however 10 µM AuNPs in 10% FBS medium did not yield any SERS spectra under the acquisition conditions used. This could be due to limited nanoparticle uptake as well as the protein corona preventing intracellular aggregation at high serum concentration. Nevertheless, the other AuNP concentrations under 10% FBS conditions allowed observation of high SERS signals. Internalisation of AuNPs inside cells was confirmed by comparison of intracellular SERS spectra with those obtained from control AuNPs incubated in each serum condition in the absence of cells (Supporting Information **Figures S3A-B**). The SERS spectra from control AuNPs show peaks arising from proteins which likely form a corona around them. The intracellular SERS spectra have understandably some similarities with that obtained from control AuNPs as mostly proteins would be adsorbed. Crucially though intracellular spectra have less distinct individual peaks as other molecules in the immediate environment of NPs would contribute and superpose on the protein corona peaks to yield a much more complex pattern. Furthermore, the protein corona around a NP is subject to dynamic compositional changes through molecular exchange with its environment. Therefore even though SERS measurements may report primarily the corona they would interrogate the changing conditions.

Mean spectra representing cells exposed to each different treatment of AuNP concentrations and media-serum composition (**Figures 3A,C**) show spectral variation between them while showing typical cellular Raman peaks. These include peaks at 500 cm^{-1} (protein cross-links), 642 cm^{-1} (Tyr/Phe), 677 cm^{-1} (DNA bases), 813 cm^{-1} (RNA/nuc acids), 1000 cm^{-1} and 1030 cm^{-1} (Phe), 1160-70 cm^{-1} (collagen/lipids), 1240-80 cm^{-1} (amide III) and 1550-60 cm^{-1} (amide II). A full list of tentative spectral assignments can be found in the Supporting Information at table 1**.**

While spectral variation is clear between cells administered with different AuNP concentrations both in 1% and 10% FBS-media, this observation by itself does not implicate AuNP treatment (internalisation) as a cause (or as a trigger to cause) for the differences. Varying media-serum content has been reported to alter intracellular localisation of AuNPs as a result of varying protein corona make-up, with decreased enrichment of protein corona found to increase the likelihood of NPs evading endolysosomal vesicles to achieve free cytosolic residence[23]. Due to the sensitivity of intracellular SERS measurements, sampling from different cellular locations can give drastically different spectral signatures and has been used as such for cellular characterisation and mapping[7,47–49].

In order to distinguish between spectral variations that might arise due to location of AuNPs from those possibly arising from nanoparticle internalisation and concomitant stress induced, understanding of how similar or different spectra are within and between different treatments was required. Spectral differences arising from increased AuNP treatment concentrations are subtle. PCA was therefore performed on the data from cells within each media serum composition. The results presented in **Figure 3B,D** show the extent of segregation observed in PC1 scores. PC1 represents the component which accounts for the largest variance within the dataset, taking values of 60.7 and 71.1% for 1 and 10% FBS treatments, respectively. The variance accounted for by higher order PCs incrementally decreases with their generation. Spectra collected from cells with AuNPs administered in 10% FBS media (**Figure 3D**, blue) form two clusters, the largest of which located at PC1 value -0.92 and to lesser extent at PC1 = 0.85. The cluster at PC1 score of -0.92 exhibits a tighter clustering of points than that at 0.85. The PC1 distributions of scores corresponding to spectra from 100 and 250 μM AuNP incubation concentrations under high serum (10%) conditions are fairly consistent. A subtle, yet notable observation is an increased clustering of scores at PC1 = 0.85 in cells incubated with 250 μM compared to 100 μM AuNPs. The observation of two clear regions of clustering may indicate that spectral differences between the clusters could be attributed to cellular location or some other effect, but the altered distribution of scores between the two clusters with AuNP concentration may be due to spectral variation caused by cellular events due to increased NP uptake. The subtlety of this effect, as only observed through statistical analysis does not correlate with the results of the DCF-DA assay (**Figure 2B**) which do not show much change between 100 and 250 μM treatments at 10% serum conditions. This also implies that the alteration of SERS spectra on increased internalisation of NPs is more complex and not just attributable to a simple increase of ROS generation and resultant oxidative stress.

Spectra obtained from cells incubated with AuNPs in media containing 1% FBS exhibit a more pronounced effect of AuNP concentration-dependent shifts in PC1 score distribution (**Figure 3B**, red). The clustering of scores at PC1 = 0.92 is consistent across 10, 100 and 250 μM AuNP treatments and decreases with concentration. Spectra acquired from cells incubated with 250 μM AuNPs exhibit a shifted distribution, towards a larger peak in scores at PC1 = -0.88. This shift in distribution is similarly seen for 100 μM treatments, displaying a secondary peak in score distribution at PC1 = -0.35, suggesting the accentuation of some SERS spectral effect, which tends towards the clustering at PC1 = -0.88 in a NP concentration-dependent manner. The trend in PC scores correlates well with the results of the DCF-DA assay which shows incremental increase on increasing AuNP treatment concentrations in 1% FBS. This suggests that ROS generation is at the very least one consequence of greater internalisation of AuNPs. Thus the trend in PC1 scores distribution of SERS spectra for AuNP treatments with increasing concentrations is similar in both 1% and 10% FBS media but crucially the corresponding ROS assay results are only pronounced for 1% FBS conditions. This is testament to both the complexity of the relationship between NP uptake and molecular-level changes induced in cells and also the increased sensitivity of SERS-PCA experimentation compared to fluorescence assays.

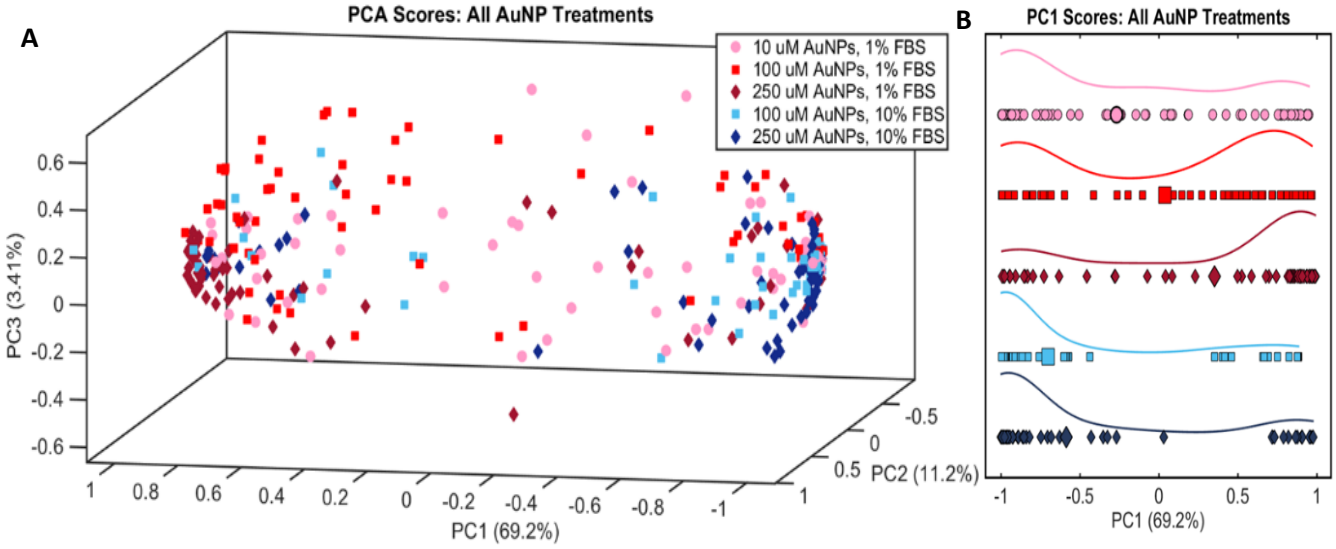

Figure 4 PCA analysis performed on the AuNP-treated SERS spectra as a single dataset. PCA scores demonstrate SERS spectra collected from cells treated with 10 µM AuNPs in 1 % FBS (pink circles) to share more features with those treated with 100 and 250 µM in 10 % FBS (light and dark blue squares and diamonds respectively) in A) 3 and B) 1 dimensional scatterplots. PC1 scores suggest an AuNP-dependent variation in the SERS spectral characteristics within the 1 % FBS treatments.

The trend observed with PCA of SERS spectra for both 1% and 10% considered separately (**Figure 3**) was explored further by carrying out PCA on the dataset in its entirety, combining both media-serum conditions and all AuNP treatment concentrations (**Figures 4A-B**). New insights are provided as the PCA calculation is run taking more data into consideration, generating new axes in PC space (PCs) to those previous and thus new comparisons. Observation of scores in 3 dimensions (PCs1-3, **Figure 4A**) is complex but nevertheless displays that the data clusters around two major PC1 score values of 0.78 and -0.92, which are dominated by data points from 250 µM/10% FBS and 250 µM/1% FBS treatments, respectively. Moreover, it can be seen that majority of the data points from 100 µM/10% FBS treatment are also coincident with those of 250 µM/10% FBS indicating spectral similarity between them. Similarly, a majority of the 100 µM/1% FBS treatment spectral data points align with the 250 µM/1% FBS treatment cluster. The spectral data points for the 10 µM/1% FBS treatment are however dispersed within and in between the two dominant clusters. Simplification to a single dimension which accounts for the greatest variance in the dataset (PC1, **Figure 4B**) allows observation of the trends more clearly. A significant separation is observed between spectra recorded from cells treated with AuNPs at 250 µM in 10% and 250 µM 1% serum media, forming the two previously described clusters, respectively. Again, the 100 µM/10% FBS treatment shows almost an identical scores distribution to the 250 µM/10% FBS treatment. The trend in PC score distribution and the changes are similar to those generated from PCA calculations run on each media composition separately. Furthermore, the effect is accentuated in the case of 100 µM AuNP treatment in 1% FBS media, which now shares its predominant peak in score distribution with the 250 µM/1% FBS treatment at PC1 = 0.78 having shifted away from the clustering at PC1 = -0.92, shared with the low concentration treatment. This supports the idea of AuNP dose-dependent changes of the molecular environment detected by our SERS measurements. Strikingly, PC1 scores reveal a clustering, and thus strong spectral resemblance, of 10 µM AuNPs in 1% FBS cell spectra with those of the 100 µM and 250 µM in 10% FBS treated cells at PC1 = -0.92. These cannot be attributed to changes to the corona itself (which will be thicker in the 10% serum case). However, it is possible that the degree of cellular internalisation is similar in these cases and therefore they induce similar cellular changes accounting for spectral similarity shown by the PCA analysis in **Figure 4**. Therefore, we investigated the internalisation of AuNPs under all the conditions both qualitatively and quantitatively to find out whether high serum treatments reduced uptake into cells.

AuNP Doses and Uptake

To understand the dose dependence of the SERS spectra and PC analysis it was important to verify the actual internalisation. Therefore, confocal microscopy and ICP-MS were performed on cell-NP preparations in order to image AuNP distribution (**Figure 5**) and quantify internalisation (**Figure 6**), respectively.

Cellular internalisation was imaged by scattering of AuNPs (green) within cells stained by CellTracker (red), confirming their residence inside cells. 3D cross-sections of representative cells are shown in **Figures 5A-F**. 10 µM AuNP treatment in 1% serum media (**Figure 5A**) shows only a small amount of AuNPs inside a clearly healthy cell (showing near complete staining and membrane features). A trend of increasing NP internalisation was observed as treatment concentrations were increased in 1% serum media (**Figures 5C,E**), accompanied by visible signs of cell stress (incomplete staining, disruption of membranes, enlargement of nucleus). Treatment in 10% serum media (**Figures 5B D,F**) however shows cells which appear significantly less damaged than the corresponding NP dose in 1% media. The damage observed in 1% serum conditions correlates to the increased ROS generation detected by DCF-DA assay. Small accumulations of AuNPs were observed at cellular membranes, adhered to the outside of the cell or undergoing internalisation at time of fixing, at high concentrations of dosage; however the majority of AuNPs are internalised within cells. Confocal images qualitatively confirm that internalisation of AuNPs occurs in all conditions. However, to quantitate the amount of AuNP uptake ICP-MS measurements were carried out.

Quantification of AuNP uptake was achieved by ICP-MS of control and NP-incubated cells following washing, lysing and dissolution of cellular and NP material in aqua regia. The concentration of Au detected in the digested cellular material demonstrated increased uptake (ten-fold between 10 and 250 µM treatments) of AuNPs

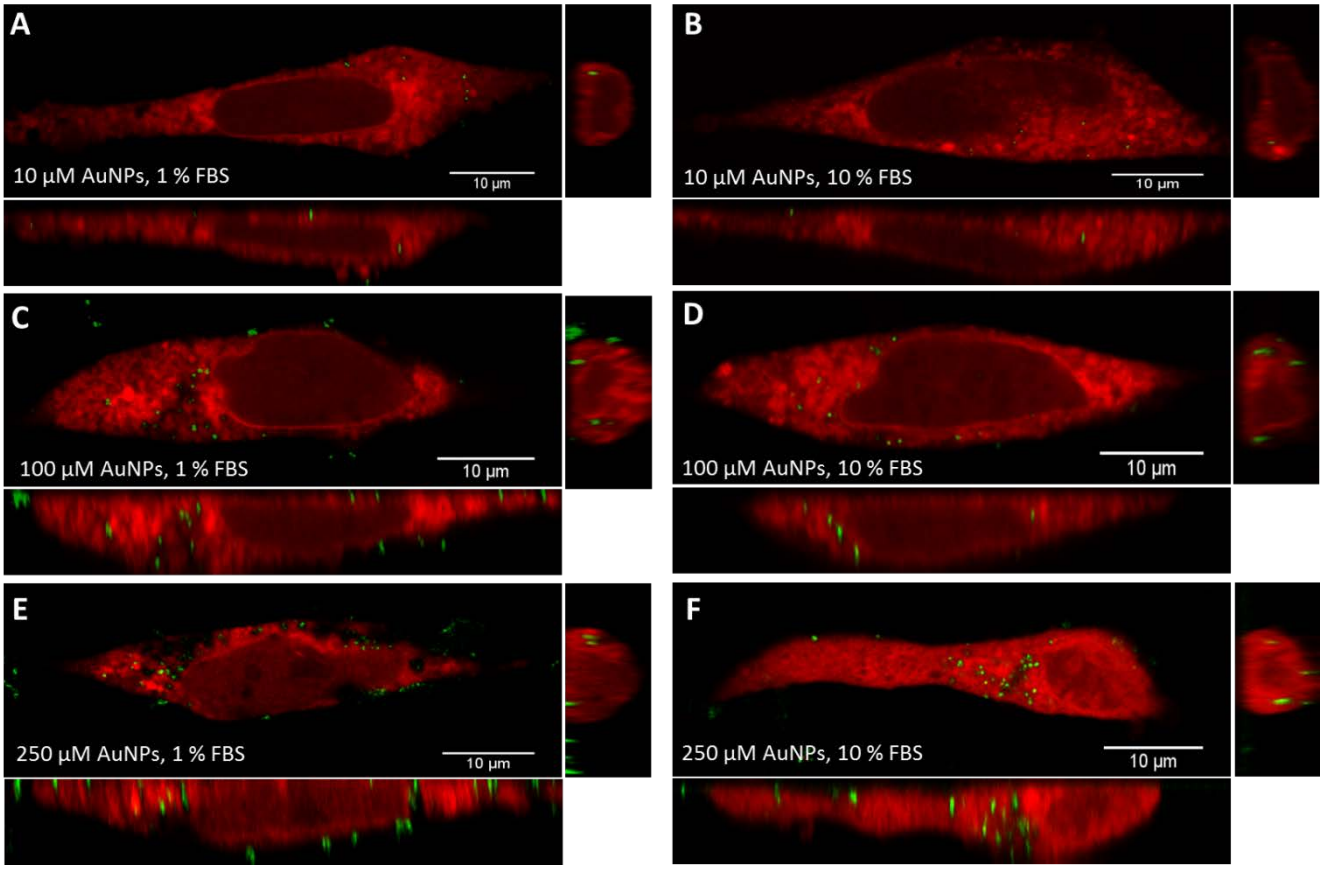

Figure 5 Verification of internalisation of AuNPs (green) in cells (red) by 3D confocal microscopy. A central slice of a representative cell with corresponding orthogonal sections are shown with increasing concentrations (A) 10 µM (C) 100 µM and (E) 250 µM under reduced serum (1%) treatment and at (B) 10 µM (D) 100 µM and (F) 250 µM under high serum (10%) conditions are shown. The number of nanoparticles inside cells increases with increasing AuNP dose concentration. The cells treated under 10% serum condition are visibly healthier even at a high dose of 250 µM. The cells were stained with the fluorescent dye celltracker red to visualise the cytoplasm and the cell contour. The AuNPs were imaged using their scattering with a 514 nm laser excitation and celltracker fluorescence was excited by a 561 nm laser excitation.

with increased incubation concentration in both 1% and 10% serum media compositions (**Figure 6**). Comparison of uptake in different media compositions reveals vastly increased concentrations of Au under 1% FBS conditions. 250 µM NP treatment in 1% serum media gives a mean cellular Au concentration of 101.2 µM compared to 10.4 µM in 10% serum incubation media. The reduced NP uptake in 10% media conditions supports our postulation (SERS-PCA results) above that the similarities observed in SERS spectra between 10 µM AuNP treatment in 1% serum and higher NP doses in 10% serum media treatment are indeed a result of similar extents of NP internalisation (0.95 and 2.55 µM for 10 µM/1% and 100 µM/10% treatments respectively). Thus, the observation of increasing level of NP uptake with treatments at high doses in 1% serum media, which correlates to variation in corresponding SERS spectra and PC analysis (**Figures 3 & 4**), confirms that the changes are indeed nanoparticle-concentration dependent and induced by nanoparticle exposure.

Characterising AuNP induced SERS Spectral Variation

Taking into account the spectral resemblance of cells treated with 10 µM AuNPs in 1% FBS media with cells undergoing similar degrees NP internalisation (10% FBS treatments) and comparing their spectral features with those exhibiting largest uptake (250 µM AuNPs in 1% media) can help identify SERS-markers of AuNP-induced changes (**Figure 7**). Observation of PC1 scores generated from the three treatment classes (**Figure 7B**) demonstrated that there is least spectral similarity between cells treated with 10 and 250 µM AuNPs in 1% serum-media, respectively, and can be attributed be caused by increased AuNP internalisation. Differences between the mean spectra of these classes (**Figure 7C**), and thus the effect of increased AuNP internalisation, were more closely studied to delineate potential cellular events accompanying NP-induced changes. Tentative assignment of the variations arising in cellular SERS spectra is performed in **Figure 7D** with peak intensity increases and decreases highlighted in dark and light grey shades, respectively. We point out the major spectral differences and discuss their assignment below.

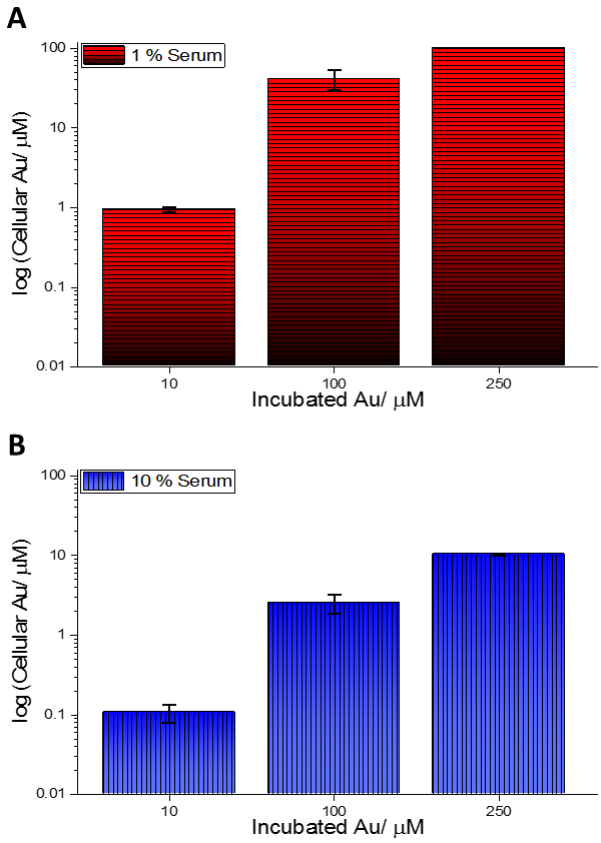

Figure 6. Quantification of AuNP uptake by ICP-MS. Intracellular concentrations of Au following treatment in low (1%) serum (A) and high (10%) serum (B) conditions are shown. The uptake amount in low serum conditions is an order of magnitude higher than the corresponding treatment under high serum conditions. Note that the y-axis is a log-scale.

We observe a flattening of S-S stretching vibration regions (540-500 cm^{-1}) which implies the destabilisation of protein folding by the breaking of cysteine-cysteine bonds; it is clear following 250 µM AuNP treatment and is in agreement with previous cell stress studies[11,12]. Conversely, the intensity of the C-C ring breathing vibration in Phe (1000 cm^{-1}) and that of its acidified form (1030 cm^{-1})[12] undergo little change between the treatments. Elevated intensities of peaks are seen within the amide III (1200-1260 cm^{-1}) and amide II (1560-1580 cm^{-1}), arising from coupling of C-N stretching and N-H bending vibrations[50]. Increased intensity of amide I C=C/C=O stretching (1601 cm^{-1}) in Phe/proteins was also observed with increased AuNP uptake. Thus, supported by the observation of decreased disulphide bridging, the unfolding of proteins arising from AuNP-induced denaturation could be inferred[11,50].

The increased peak intensity located at 1241 cm^{-1} may also correspond to protein denaturation through exposure of glycine (Gly) backbones and Pro sidechains, or asymmetrical stretching of PO_2^- from phosphodiester groups of nucleic acids. Other RNA peaks however manifest at 802 and 811 cm^{-1} (uracil-based ring breathing and O-P-O str respectively)[50] and present decreased intensities following high degrees of AuNP internalisation. Therefore, AuNP internalisation is proposed to play a role in the disruption of normal RNA-based cellular events such as transcription and translation. The higher intensities of these peaks may represent degradation through exposure or exchange of constituent chemical groups into NP electronic fields or protein corona respectively.

The fine vibrational peaks resolved within the amide II region (1480-1575 cm^{-1}) do not exhibit a consistent trend in SERS intensity changes following increased AuNP uptake. Increases may suggest exposure of coupled C-N and N-H vibrations to AuNPs and thus protein denaturation as previously described. However, the increased intensity of 1572 cm^{-1} has also been reported to arise from ring breathing vibrations in NADH[50,51], with its phosphorylated form NADPH known to provide a reductive environment for the cells to nullify increased ROS during oxidative stress[52]. The increased intensity of vibration 1562 cm^{-1} may support this, with the peak corresponding to vibrations in tryptophan (Trp), converted to quinolinate, a *de novo* precursor to the pyridine ring of NAD derivatives in eukaryotic cells[53,54]. This may present SERS detection of upregulation of cellular antioxidant defences in response to AuNP internalisation. However, this may need further investigation to establish this definitively.

Within the lower wavenumber amide II range however, peaks at 1488 and 1517 cm^{-1} decreased in intensity. While C-N/N-H coupling contributes to these peaks, they may also represent C=C breathing modes in DNA bases guanine and cytosine respectively[50]. Decreased SERS intensity of DNA-attributed vibrational modes was also observed at 680 and 1090 cm^{-1}. The possibility of AuNP-induced stress causing DNA fragmentation is therefore implied, which is a well-known to occur under cell stress[2,38,39]. A similarly complex picture is presented in lipid-assigned SERS peaks. The vibrational mode at 1305 cm^{-1} relates to CH_2 deformation in lipids, with its decreased intensity inferring possible degradation of phospholipids. This cell stress event has previously been detected by SERS within HSF and A549 cell lines upon stress induced by exposure to ZnO NPs[12]. In contrast, the C-C stretching mode of acyl chains at 1134 cm^{-1} exhibited increased SERS intensities.

While it must be noted that sound conclusions on the effect of AuNP internalisation on specific cellular pathways cannot be drawn from this study alone, a requirement for greater understanding of NP-cell interactions is clearly warranted. Intracellular SERS measurements have revealed changes to the spectra acquired accompanying varying degrees of AuNP internalisation, as recognised by application of multivariate analysis techniques and is supported by internalisation data. Such changes which are tentatively assigned to NP-induced cell stress events such as protein misfolding and denaturation, oxidation of proteins and lipids and changes to DNA/RNA regulation/structure. However, the investigation of their underlying biomechanistic causes that are either induced by or triggered by increased nanoparticle uptake are beyond the scope of this study. Significant conclusions detailing NP-induced effects on specific pathways can only be drawn after further exhaustive examination of increased sample sizes and diversity of AuNP treatments (including NP morphology, diameter, incubation period, surface modifications and cell lines).

Conclusions

The presented study has combined biological assays for cell viability and ROS detection with intracellular SERS measurements to evaluate potential perturbation of healthy cellular activity induced in human neuroblastoma cells by AuNP nanosensors. The NP dose-dependent increase in ROS generation observed by DCF-DA assay was especially not reflected in the viability results. This suggests that just measuring viability is not enough to qualify the 'internal

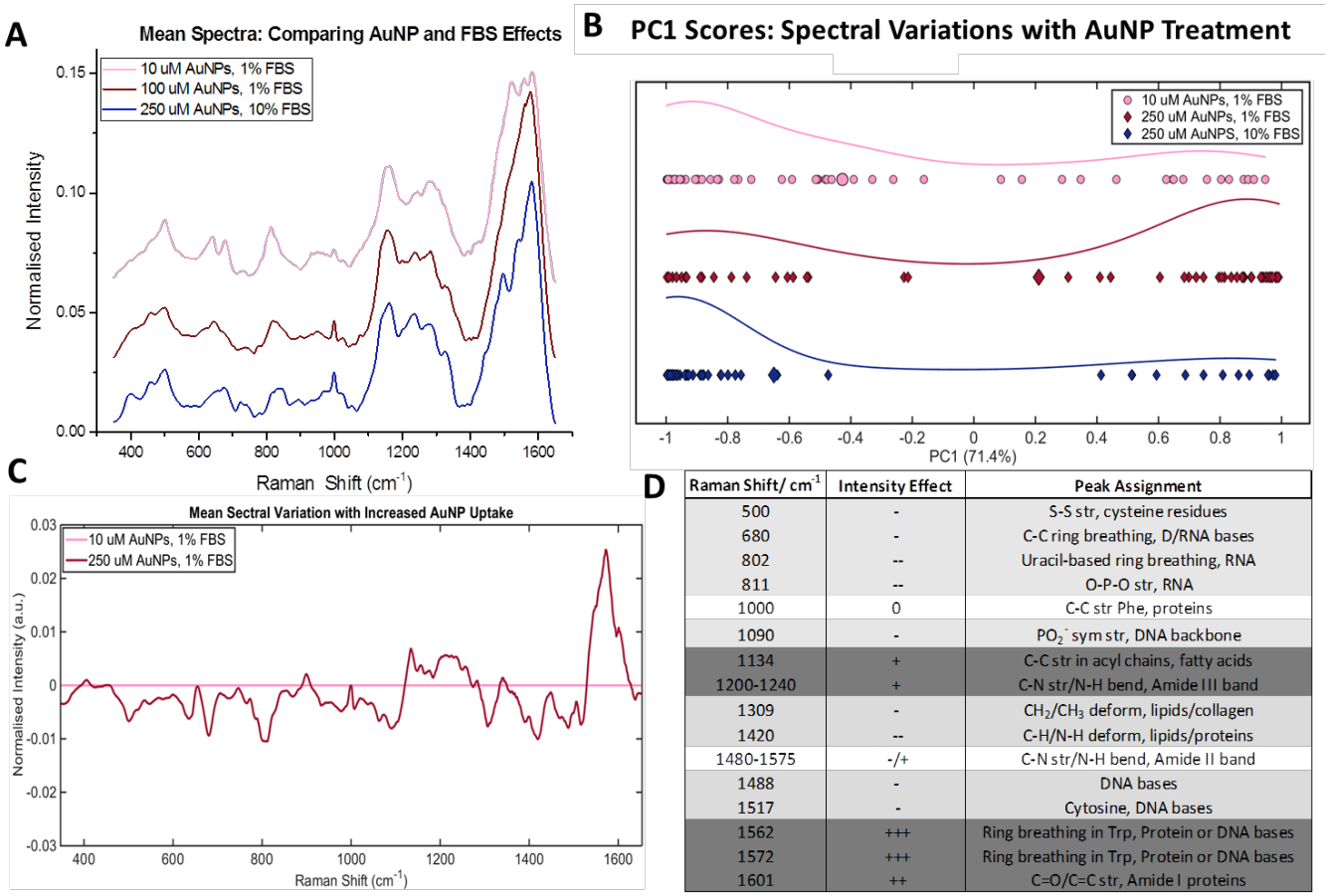

D

Raman Shift/ cm^{-1}	Intensity Effect	Peak Assignment
500	-	S-S str, cysteine residues
680	-	C-C ring breathing, D/RNA bases
802	--	Uracil-based ring breathing, RNA
811	--	O-P-O str, RNA
1000	0	C-C str Phe, proteins
1090	-	PO_2^- sym str, DNA backbone
1134	+	C-C str in acyl chains, fatty acids
1200-1240	+	C-N str/N-H bend, Amide III band
1309	-	CH_2/CH_3 deform, lipids/collagen
1420	--	C-H/N-H deform, lipids/proteins
1480-1575	-/+	C-N str/N-H bend, Amide II band
1488	-	DNA bases
1517	-	Cytosine, DNA bases
1562	+++	Ring breathing in Trp, Protein or DNA bases
1572	+++	Ring breathing in Trp, Protein or DNA bases
1601	++	C=O/C=C str, Amide I proteins

Figure 7. Identification of nanoparticle induced spectral changes. (A) Spectra comparing AuNP dose concentration and serum conditions. The spectra are offset for clarity. (B) Shows the PC1 scores distribution for selected treatments which show similarity (10 µM/1% FBS and 250 µM/10% FBS) and most difference (250 µM/1% FBS). (C)Shows the NP-dose dependent differences in the mean SERS spectra. The mean spectrum of 10 µM/1% FBS is subtracted from both the mean spectra of both high - 250 µM/1% FBS (dark red) and low - 10 µM/1% FBS (pink) nanoparticle treatments. The main peaks in the difference spectra are tentatively assigned in (D).

health' of the cell. Further SERS measurements and PCA analysis revealed that altered spectral characteristics in cells treated with increased doses of AuNPs in low serum media, can be concluded to be a result of increased AuNP internalisation as confirmed by ICP-MS. Serum-rich conditions led to lower internalisation in general and comparable to low dosage at reduced serum conditions. This resulted in spectra under high serum conditions to be similar to those at low dosage under reduced serum conditions, again confirming that spectral changes we observe are indeed due to increased internalisation of AuNPs. Confocal imaging of AuNPs within cells verified NP internalisation further to confirm that SERS spectra were being collected from inside cells. Correlative information provided by DCF-DA ROS assay identified that oxidative stress plays some role in the complex spectral changes observed following excessive NP uptake by cells. Assignment of spectral variations arising from AuNP-induced stress identified SERS peaks which have been previously attributed to oxidative stress following administration of other inorganic NPs, such as protein denaturation and misfolding events, lipid decomposition and DNA fragmentation[11,12]. Thus, overall our study shows that nanosensors themselves can perturb the environment which they measure and therefore care must be taken in the application of NPs, including AuNPs, for intracellular SERS investigations. Their high uptake causes changes in their biochemical environment, which is a deviation from the 'natural' cellular state, and thus affects SERS spectra. Although the changes are unarguably complex and need to be better understood, oxidative stress as one of the effects cannot be ruled out. Therefore, we open discussion on the standardisation of intracellular nanosensing methodologies. This is crucial for the validity of intracellular SERS experiments, the understanding and insight it offers regarding molecular pathways and NP-cell interactions and for all arising applications of intracellular SERS.

Acknowledgements

Support from the Institute for Life Sciences (IFLS), University of Southampton, ERC grant NanoChemBioVision 638258 and BBSRC iCase BB/N50404X/1 award with Astra Zeneca are kindly acknowledged.

Notes and references

1 J. Taylor, A. Huefner, L. Li, J. Wingfield and S. Mahajan, *The Analyst*, 2016, **141**, 5037–5055.

2 P. Khanna, C. Ong, B. Bay and G. Baeg, *Nanomaterials*, 2015, **5**, 1163–1180.

3 Y. S. Huh, A. J. Chung and D. Erickson, *Microfluid. Nanofluidics*, 2009, **6**, 285–297.

4 C. A. R. Auchinvole, P. Richardson, C. McGuinnes, V. Mallikarjun, K. Donaldson, H. McNab and C. J. Campbell, *ACS Nano*, 2012, **6**, 888–896.

5 J. Ando, K. Fujita, N. I. Smith and S. Kawata, *Nano Lett.*, 2011, **11**, 5344–5348.
6 J. Ando, T. Yano, K. Fujita and S. Kawata, *Phys. Chem. Chem. Phys.*, 2013, **15**, 13713.
7 A. Huefner, W.-L. Kuan, K. H. Müller, J. N. Skepper, R. A. Barker and S. Mahajan, *ACS Nano*, 2015, **10**, 307–316.
8 K. A. Hollywood, I. T. Shadi and R. Goodacre, *J. Phys. Chem. C*, 2010, **114**, 7308–7313.
9 I. A. Larmour and D. Graham, *The Analyst*, 2011, **136**, 3831.
10 M. F. Escoriza, J. M. VanBriesen, S. Stewart and J. Maier, *Appl. Spectrosc.*, 2007, **61**, 812–823.
11 B. Kang, L. A. Austin and M. A. El-Sayed, *ACS Nano*, 2014, **8**, 4883–4892.
12 G. Kuku, M. Saricam, F. Akhatova, A. Danilushkina, R. Fakhrullin and M. Culha, *Anal. Chem.*, , DOI:10.1021/acs.analchem.6b02917.
13 W. Wang, L. Zhang, L. Li and Y. Tian, *Anal. Chem.*, 2016, **88**, 9518–9523.
14 B. Kang, L. A. Austin and M. A. El-Sayed, *Nano Lett.*, 2012, **12**, 5369–5375.
15 Y. H. Ong, M. Lim and Q. Liu, *Opt. Express*, 2012, **20**, 25041.
16 Ö. F. Karataş, E. Sezgin, Ö. Aydın and M. Çulha, *Colloids Surf. B Biointerfaces*, 2009, **71**, 315–318.
17 B. Kang, M. M. Afifi, L. A. Austin and M. A. El-Sayed, *ACS Nano*, 2013, **7**, 7420–7427.
18 K. Ock, W. I. Jeon, E. O. Ganbold, M. Kim, J. Park, J. H. Seo, K. Cho, S.-W. Joo and S. Y. Lee, *Anal. Chem.*, 2012, **84**, 2172–2178.
19 J. Yang, Z. Wang, S. Zong, H. Chen, R. Zhang and Y. Cui, *Biosens. Bioelectron.*, 2014, **51**, 82–89.
20 J. Song, J. Zhou and H. Duan, *J. Am. Chem. Soc.*, 2012, **134**, 13458–13469.
21 A. M. Alkilany and C. J. Murphy, *J. Nanoparticle Res.*, 2010, **12**, 2313–2333.
22 M. P. Monopoli, A. S. Pitek, I. Lynch and K. A. Dawson, *Methods Mol. Biol. Clifton NJ*, 2013, **1025**, 137–155.
23 P. I. T. Thomson and C. J. Campbell, in *Nanoscale Sensors*, eds. S. Li, J. Wu, Z. M. Wang and Y. Jiang, Springer International Publishing, Cham, 2013, vol. 19, pp. 35–54.
24 M. P. Monopoli, D. Walczyk, A. Campbell, G. Elia, I. Lynch, F. Baldelli Bombelli and K. A. Dawson, *J. Am. Chem. Soc.*, 2011, **133**, 2525–2534.
25 J. S. Gebauer, M. Malissek, S. Simon, S. K. Knauer, M. Maskos, R. H. Stauber, W. Peukert and L. Treuel, *Langmuir*, 2012, **28**, 9673–9679.
26 M. Lundqvist, J. Stigler, T. Cedervall, T. Berggård, M. B. Flanagan, I. Lynch, G. Elia and K. Dawson, *ACS Nano*, 2011, **5**, 7503–7509.
27 M. Mahmoudi, J. Meng, X. Xue, X. J. Liang, M. Rahman, C. Pfeiffer, R. Hartmann, P. R. Gil, B. Pelaz, W. J. Parak, P. del Pino, S. Carregal-Romero, A. G. Kanaras and S. Tamil Selvan, *Biotechnol. Adv.*, 2014, **32**, 679–692.
28 R. Lévy, U. Shaheen, Y. Cesbron and V. Sée, *Nano Rev.*, , DOI:10.3402/nano.v1i0.4889.
29 S. Schlücker, *Angew. Chem. Int. Ed.*, 2014, **53**, 4756–4795.
30 S. Schlücker, *ChemPhysChem*, 2009, **10**, 1344–1354.
31 K. A. Willets, *Anal. Bioanal. Chem.*, 2009, **394**, 85–94.
32 S. J. Soenen, P. Rivera-Gil, J.-M. Montenegro, W. J. Parak, S. C. De Smedt and K. Braeckmans, *Nano Today*, 2011, **6**, 446–465.
33 M. A. Vetten, N. Tlotleng, D. Tanner Rascher, A. Skepu, F. K. Keter, K. Boodhia, L.-A. Koekemoer, C. Andraos, R. Tshikhudo and M. Gulumian, *Part. Fibre Toxicol.*, 2013, **10**, 50.
34 E. Birben, U. M. Sahiner, C. Sackesen, S. Erzurum and O. Kalayci, *World Allergy Organ. J.*, 2012, **5**, 9–19.
35 B. Halliwell, *Biochem. Soc. Trans.*, 2007, **35**, 1147–1150.
36 J. J. Li, L. Zou, D. Hartono, C.-N. Ong, B.-H. Bay and L.-Y. Lanry Yung, *Adv. Mater.*, 2008, **20**, 138–142.
37 A. Avalos, A. I. Haza, D. Mateo and P. Morales, *J. Appl. Toxicol.*, 2014, **34**, 413–423.
38 N. Singh, B. Manshian, G. J. S. Jenkins, S. M. Griffiths, P. M. Williams, T. G. G. Maffeis, C. J. Wright and S. H. Doak, *Biomaterials*, 2009, **30**, 3891–3914.
39 D. Ali, S. Alkahtani, M. A. Al Gurabi and S. Alarifi, *OncoTargets Ther.*, 2015, 295.
40 T. Finkel and N. J. Holbrook, *Nature*, 2000, **408**, 239–247.
41 M. Schieber and N. S. Chandel, *Curr. Biol.*, 2014, **24**, R453–R462.
42 J. Jiang, C. Auchinvole, K. Fisher and C. J. Campbell, *Nanoscale*, 2014, **6**, 12104–12110.
43 A. Huefner, W.-L. Kuan, R. A. Barker and S. Mahajan, *Nano Lett.*, 2013, **13**, 2463–2470.
44 J. Kovalevich and D. Langford, in *Neuronal Cell Culture*, eds. S. Amini and M. K. White, Humana Press, Totowa, NJ, 2013, vol. 1078, pp. 9–21.
45 A. Shamsaie, J. Heim, A. A. Yanik and J. Irudayaraj, *Chem. Phys. Lett.*, 2008, **461**, 131–135.
46 J. Trevisan, P. P. Angelov, A. D. Scott, P. L. Carmichael and F. L. Martin, *Bioinformatics*, 2013, **29**, 1095–1097.
47 A. Huefner, D. Septiadi, B. D. Wilts, I. I. Patel, W.-L. Kuan, A. Fragniere, R. A. Barker and S. Mahajan, *Methods*, 2014, **68**, 354–363.
48 Y. Chen, X. Bai, L. Su, Z. Du, A. Shen, A. Materny and J. Hu, *Sci. Rep.*, 2016, **6**, 19173.
49 J. Kneipp, H. Kneipp, M. McLaughlin, D. Brown and K. Kneipp, *Nano Lett.*, 2006, **6**, 2225–2231.
50 Z. Movasaghi, S. Rehman and I. U. Rehman, *Appl. Spectrosc. Rev.*, 2007, **42**, 493–541.
51 R. Malini, K. Venkatakrishna, J. Kurien, K. M. Pai, L. Rao, V. B. Kartha and C. M. Krishna, *Biopolymers*, 2006, **81**, 179–193.
52 R. Singh, R. J. Mailloux, S. Puiseux-Dao and V. D. Appanna, *J. Bacteriol.*, 2007, **189**, 6665–6675.
53 O. Kurnasov, V. Goral, K. Colabroy, S. Gerdes, S. Anantha, A. Osterman and T. P. Begley, *Chem. Biol.*, 2003, **10**, 1195–1204.
54 F. Sahm, I. Oezen, C. A. Opitz, B. Radlwimmer, A. von Deimling, T. Ahrendt, S. Adams, H. B. Bode, G. J. Guillemin, W. Wick and M. Platten, *Cancer Res.*, 2013, **73**, 3225–3234.

